Argon Adsorption on MCM-41 Mesoporous Crystal Studied by In Situ Synchrotron Powder X-ray Diffraction

Norihiro Muroyama,[†] Arisa Yoshimura,[‡] Yoshiki Kubota,[‡] Keiichi Miyasaka,[†] Tetsu Ohsuna,[§,||] Ryong Ryoo,[⊥] Peter I. Ravikovitch,[#] Alexander V. Neimark,*[,∇] Masaki Takata,[○] and Osamu Terasaki*[,†]

Structural Chemistry, Arrhenius Laboratory, Stockholm University, SE-10691 Stockholm, Sweden, Department of Physical Science, Graduate School of Science, Osaka Prefecture University, 1-1 Gakuen-cho, Naka-ku, Sakai, Osaka 599-8531, Japan, CREST, Japan Science and Technology Agency, Honcho 4-1-8, Kawaguchi-shi, Saitama, 332-0012, Japan, Kagami Memorial Laboratory for Materials Science and Technology, Waseda University, Nishiwaseda 2-8-26, Shinjuku-ku, Tokyo, 169-0051, Japan, Center for Functional Nanomaterials and Department of Chemistry (School of Molecular Science BK21), Korea Advanced Institute of Science and Technology, Daejeon, 305-701, Korea, ExxonMobil Research and Engineering Company, 1545 Route 22 East, Annandale, New Jersey 08801, Department of Chemical and Biochemical Engineering, Rutgers, The State University of New Jersey, 98 Brett Road, Piscataway, New Jersey 08854-8058, and Structural Science Laboratory, Harima Institute SPring-8 Center, RIKEN and CREST, Japan Science and Technology Agency, Sayo-gun, Hyogo, 679-5198, Japan

Received: January 15, 2008; Revised Manuscript Received: April 2, 2008

Equilibrium argon adsorption from the gas phase on mesoporous MCM-41 silica of hexagonal structure is directly studied by in situ synchrotron powder X-ray diffraction (XRD) measurements at SPring-8. The diffraction intensity data is analyzed by extending the previously developed analytical formula for the crystal structure factors of MCM-41 to account for argon adsorbed in the pores. It is clearly observed that argon adsorbs in layers on the pore walls at low gas pressures and exhibits sudden capillary condensation as the gas pressure increased. The proposed method of interpretation of XRD data allows one to calculate the density ratio between the silica wall and condensed argon, the pore size, and the pore wall fluctuation/roughness, together with the thickness of the adsorbed layer as a function of the gas pressure. The results of in situ XRD experiments are compared with the results of argon adsorption volumetric experiments. The adsorption data are interpreted with the quench solid density functional theory (QSDFT), which takes into account the pore wall roughness. The perfect agreement of the QSDFT isotherm predicted from the adsorption data and the XRD recalculated isotherm suggests that the adsorption porosimetry and XRD measurements can be reconciled provided a proper interpretation of the experimental data.

Introduction

Using the self-organizing mechanism of amphiphilic molecules in a water/silica system, many different mesoporous materials have been synthesized[1–5] aimed at various technical applications such as catalysis, separation processes, and drug delivery. Structural characterization of mesoporous materials is essential for understanding their properties and also for designing novel materials for specific purposes. The channels, cages, or pores, which are formed within the amorphous silica matrix, are arranged periodically in space, forming a regular pore network with a well-defined crystallographic symmetry. Therefore, one can apply crystallographic techniques to the structural analysis. To emphasize this feature, we use the term "mesoporous crystal", although the silica matrix is amorphous. Powder X-ray diffraction (XRD), transmission electron microscopy (TEM), and gas adsorption experiments are the main tools for the structural characterization of mesoporous crystals. Among them, XRD is one of the most quantitative techniques, while the gas adsorption, which provides the pore size, pore volume, and surface area, is a standard characterization technique, called adsorption porosimetry. However, the underlying mechanisms of adsorption and desorption are still under discussion. Assumptions employed for calculating the structural parameters from adsorption isotherms are made differently depending on the pore geometries. Capillary condensation, which is a vapor−liquid phase transformation in a confined geometry, strongly depends on both the pore geometry and the fluid−fluid and fluid−solid intermolecular interactions. Thus, it is highly desirable to devise an independent experimental technique for in situ studies of gas adsorption on mesoporous materials, which can be employed for examination and validation of the results of adsorption porosimetry.

The electron crystallographic (EC) approach we previously developed is the only available method for solving three-dimensional (3D) structures of ordered mesoporous silica crystals at present.[6,7] An electrostatic potential density map determined from a set of high-resolution transmission electron microscope (HRTEM) images must be transformed to the silica

* Corresponding author. E-mail: terasaki@struc.su.se; fax: +46-8-163118; Phone: +46-8-162379 (O.T.). E-mail: aneimark@rutgers.edu (A.V.N.).
[†] Stockholm University.
[‡] Osaka Prefecture University.
[§] CREST, Japan Science and Technology Agency.
[||] Waseda University.
[⊥] Korea Advanced Institute of Science and Technology.
[#] ExxonMobil Research and Engineering Company.
[∇] Rutgers, The State University of New Jersey.
[○] Harima Institute SPring-8 Center, Japan Science and Technology Agency.

10.1021/jp800385t CCC: $40.75
Published on Web 07/01/2008

wall structure in this analysis. This transformation requires data on both the silica density and the pore volume. Developing this EC method, we have learned that it is necessary to elaborate quantitative methods for both the diffraction-based and the gas adsorption experiments in order to reconcile the results of these techniques. It is well-known that as the vapor pressure increases, the adsorbate molecules fill the mesopores by forming adsorbed films until, at a certain pressure, a vapor−liquid transition occurs, which leads to the complete pore filling with the liquid-like adsorbate. Although this general picture of adsorption and subsequent capillary condensation in mesoporous solids is generally accepted, the details are still the subject of theoretical discussions because of the lack of additional experimental techniques.

The pore shape and the pore size of two-dimensional (2D) hexagonally ordered mesopores in MCM-41 have been studied.[8,9] There have also been several reports on in situ X-ray experiments for the study of gas adsorption processes in MCM-41 and/or SBA-15 by powder XRD,[10] X-ray absorption[11,12] or small-angle XRD intensity measurements.[10,12–15] For powder XRD studies of gas absorbed films formed within the 2D mesopores with *p6mm* symmetry, a cylindrical structure model of multidensity with step-levels, such as dense silica matrix, less dense silica with microporous corona (for the case of SBA-15), adsorbed film, and empty core, has been used.[12,14,15]

Previously, we have employed analytical structure models for as-synthesized and calcined MCM-41, and found that as-synthesized and calcined MCM-41 samples yield the diffraction data that are well-explained by the *p6mm* structures with hexagonal and circular pore shapes, respectively.[16] In the general case of structural studies of mesoporous crystals by powder X-ray and neutron diffraction experiments, the number of reflections, n, is very limited. Therefore, a simple but physically meaningful structure model with m parameters ($m \leq n$) should be employed. For the structure of mesoporous crystals with a 2D plane group of *p6mm*, the following structural parameters should be considered: (i) unit cell constant, (ii) pore shape, (iii) pore size, and (iv) projected silica wall density along the channel direction as a function of position, which can be expressed as a Gaussian function effectively.[16,17] It is natural for us to start in situ XRD intensity measurement from a relatively simple structure of MCM-41 mesoporous crystal with cylindrical pore channels (2D structure with a plane group of *p6mm*), which were confirmed by our TEM observation.[18] In this paper, we study the Ar adsorption process in the mesopores of MCM-41 crystal both by in situ powder XRD intensity and by volumetric adsorption measurements. The number of electrons in the system increases with the increasing number of Ar atoms adhering onto the mosopore walls. Using an internal standard as a diffraction intensity standard, we can measure "absolute" diffraction intensity, and therefore we can refine the structural parameters in the whole set of diffraction data obtained at different gas pressures. We show that the results of these techniques can be reconciled by using the quench solid density functional theory (QSDFT) of adsorption developed by two of us recently.[19] We will separately report an in situ Ar-gas adsorption study in the mesopores of the MCM-48 and SBA-16 crystals, which have a 3D-gyroid pore system with $Ia\bar{3}d$ symmetry and a body-centered cubic system with $Im\bar{3}m$ symmetry, respectively.

1. Structure Factor. In order to apply the analytical approach[16] for studies of the gas adsorption process, it is necessary to modify a few equations.

In kinematical scattering, the scattered intensity, $I(\mathbf{k})$, is expressed as

$$I(\mathbf{k}) \propto |F(\mathbf{k})|^2 \tag{1.1}$$

$$F(\mathbf{k}) = \int \rho(\mathbf{x}) e^{2\pi i \mathbf{k}\cdot\mathbf{x}} \mathrm{d}\mathbf{x} = \mathcal{F}[\rho(\mathbf{x})] \tag{1.2}$$

where $F(\mathbf{k})$ is a scattering amplitude, $\rho(\mathbf{x})$ is a density distribution of scattering matters, symbol $\mathcal{F}$ represents Fourier transformation, and $\mathbf{x}$ and $\mathbf{k}$ [$|\mathbf{k}| = (2 \sin \theta)/\lambda$] are a position vector in the real space and a wave vector in the reciprocal space, respectively. In general, the calculation for the operation of a product is easier than that for a convolution. A scattering intensity is a real function, and if the distribution of scattering matter is known, the scattering intensity can be calculated. On the other hand, the structure factor, $F(\mathbf{k})$, is a complex function with a phase $\varphi(\mathbf{k})$, which is dependent on a choice of the origin,

$$F(\mathbf{k}) = |F(\mathbf{k})| e^{i\varphi(\mathbf{k})}$$

The crystal $C(\mathbf{x})$ is a representation of $\rho(\mathbf{x})$ for a crystal with the functions of a basis $B(\mathbf{x})$, a lattice $L(\mathbf{x})$, and a crystal size $S(\mathbf{x})$, and is expressed as

$$C(\mathbf{x}) = B(\mathbf{x}) * [L(\mathbf{x}) \cdot S(\mathbf{x})] \tag{1.3}$$

where the symbol * indicates an operation of the convolution.

The following equation for Fourier transformation relevant to crystallography expresses the relationships between the Fourier transform and convolution:

$$\mathcal{F}[B(\mathbf{x}) * L(\mathbf{x})] = \mathcal{F}[B(\mathbf{x})] \cdot \mathcal{F}[L(\mathbf{x})]$$

Other important theorems of Fourier transformation are the relationship for Dirac's delta function, $\delta(\mathbf{x})$,

$$\mathcal{F}[\delta(\mathbf{x} - \mathbf{x}_0)] = \mathrm{e}^{2\pi i \mathbf{k}\,\mathbf{x}_0}$$

$$\mathcal{F}[\mathrm{e}^{2\pi i \mathbf{k}\,(\mathbf{x}-\mathbf{x}_0)}] = \delta(\mathbf{x} - \mathbf{x}_0)$$

The 2D crystals such as MCM-41 can be described by

$$C(\mathbf{x}) = C(\mathbf{r}, z) = C(\mathbf{r}) \cdot H(z) \tag{1.4}$$

where a 3D vector is separated into a 2D vector in the pore cross section and z the direction along the channel axis perpendicular to r; $C(\mathbf{r})$ is a function of a 2D plane crystal, and the finite length of the crystal is introduced by $H(z) = 1$ for $-Z/2 \leq z \leq Z/2$ ($H(z) = 0$ otherwise), where Z is the length of the crystal along the channel direction, z.

The crystal structure factor, $F(\mathbf{k}_\mathbf{r}, k_z)$, of the crystal $C(\mathbf{r}, z)$ is

$$F(\mathbf{k}_\mathbf{r}, k_z) = \int \mathrm{d}\mathbf{r} \int_{-Z/2}^{Z/2} \mathrm{d}z C(\mathbf{r}, z) \mathrm{e}^{2\pi i \mathbf{k}_\mathbf{r}\mathbf{r}} \mathrm{e}^{2\pi i k_z z}$$

$$= \int C(\mathbf{r}) \mathrm{e}^{2\pi i \mathbf{k}_\mathbf{r}\mathbf{r}} \mathrm{d}\mathbf{r} \cdot \int_{-Z/2}^{Z/2} H(z) \mathrm{e}^{2\pi i k_z z} \mathrm{d}z \tag{1.5}$$

$$= \mathcal{F}[C(\mathbf{r})] \cdot \mathcal{F}[H(z)] \tag{1.6}$$

where $\mathbf{k}_\mathbf{r}$ is a wave vector in the 2D reciprocal space, and k_z is a scalar component perpendicular to the 2D space. As Z approaches infinity, $\mathcal{F}[H(z)]$ becomes the delta function, $\delta(k_z)$, and we have confirmed from scanning electron microscope (SEM) and TEM images that this is the case for ordinary MCM-41 crystals. Therefore $F(\mathbf{k}_\mathbf{r}, k_z)$ can be treated as 2D $F(\mathbf{k}_\mathbf{r})$, and, for simplicity in this paper, $\mathbf{k}$ is used for $\mathbf{k}_\mathbf{r}$ hereafter, and $H(z)$ is not included.

$$F(\mathbf{k}_\mathbf{r}, k_z) = F(\mathbf{k}_\mathbf{r}) = \mathcal{F}[C(\mathbf{r})] \equiv F(\mathbf{k}) \tag{1.7}$$

2. Synchrotron Powder XRD. The sample of MCM-41 with adsorbed Ar, Ar@MCM-41, is an open system, that is, the number of atoms and hence electrons, which scatter X-rays, changes as a function of number of adsorbed Ar atoms. The powder XRD intensity for the Ar@MCM-41 system is given by

$$I(\mathbf{k}) = \text{constant} \cdot N \cdot I_{\text{incident}} \cdot Ab(\mathbf{k}) \cdot L(\theta) \cdot P(\theta) \cdot m(\mathbf{k}) \cdot |F(\mathbf{k})|^2 \quad (2.1)$$

where N, I_{incident}, θ, $L(\theta)$, $P(\theta)$, $Ab(\mathbf{k})$, $m(\mathbf{k})$, and $F(\mathbf{k})$ are the number of unit cells, the incident intensity, the scattering angle, the Lorentz, polarization, and absorption factors, the multiplicity, and the structure factor for the individual unit cells, respectively. The product of the Lorenz and polarization factors $L(\theta)\cdot P(\theta)$ depends upon the experimental condition of synchrotron XRD at the beam line BL02B2, SPring-8:

$$L(\theta) \cdot P(\theta) = \frac{1}{\sin\theta \cdot \sin 2\theta}$$

The temperature (Debye−Waller) factor is effectively included in $F(\mathbf{k})$.

In order to study the adsorption process, we have to obtain $|F(\mathbf{k})|^2$ as a function of the gas pressure. During the gas adsorption in situ XRD experiment, the amount of adsorbed molecules increases upon the gas loading, therefore $Ab(\mathbf{k})$ and $F(\mathbf{k})$ in the formula for the diffraction intensity are the functions of the number of scattering centers in the system. In the previous paper, we discussed the structure factor as normalized to the structure factor at $\mathbf{k} = 0$, that is, normalized to the total number of electrons. In this experiment, for this reason, we need to use a standard intensity, which is independent of the gas adsorption experiment. To this end, we determined the scaling factor, Scale $=$ constant$\cdot N\cdot I_{\text{incident}}\cdot Ab(\mathbf{k})$, by mixing a very crystalline material, which does not affect gas adsorption, such as Si, CeO_2, Al_2O_3, together with the sample as an internal standard. The intensity eq 2.1 can then be expressed as

$$I(k) = \text{Scale} \cdot L(\theta) \cdot P(\theta) \cdot [\, m(\mathbf{k}) \cdot |F(\mathbf{k})|^2 + m_{\text{std}}(\mathbf{k}) \cdot |F_{\text{std}}(\mathbf{k})|^2] \quad (2.2)$$

where $m_{\text{std}}(\mathbf{k})$ and $F_{\text{std}}(\mathbf{k})$ are the multiplicity and the structure factor of the crystal used as the internal standard, respectively. The diffraction intensities from the sample and the internal standard, $I(\mathbf{k})$ and $I_{\text{std}}(\mathbf{k})$, do not interfere with each other; they are measured simultaneously for various values of $\mathbf{k}$. From the measurement of $I_{\text{std}}(\mathbf{k})$ at different adsorption conditions, we can obtain the factor Scale and, consequently, $|F(\mathbf{k})|^2$ as a function of adsorption.

3. Structural Model. For a calcined MCM-41, $C(\mathbf{r})$, has periodic pores, $B(\mathbf{r})$, on an infinite 2D hexagonal lattice, $L_h(\mathbf{r})$, which is restricted to a 2D hexagonal crystal shape, $S(\mathbf{r})$, and $\mathbf{r}$ is spanned in two dimensions as $\mathbf{r} = r_a\mathbf{a} + r_b\mathbf{b}$, where $|\mathbf{a}| = |\mathbf{b}| = a$ denotes a lattice constant. The internal angle $\gamma = 2\pi/3$.

$$C(\mathbf{r}) = \rho_{\text{wall}} \cdot [S(\mathbf{r}) - B(\mathbf{r}) * \{L_h(\mathbf{r}) \cdot S(\mathbf{r})\}] \quad (3.1)$$

where ρ_{wall} is the silica wall density. Boundaries between the pores and the pore walls are not sharp and smooth, so it is reasonable to introduce a fluctuation or gradient factor, which accounts for the pore surface roughness and smoothes the average density along the channel direction. The fluctuation factor is introduced by a projected function $G(\mathbf{r})$, then eq 3.1 becomes

$$C(\mathbf{r}) = \rho_{\text{wall}} \cdot [S(\mathbf{r}) - G(\mathbf{r}) * B(\mathbf{r}) * \{L_h(\mathbf{r}) \cdot S(\mathbf{r})\}] \quad (3.2)$$

For Ar@MCM-41, $C(\mathbf{r})$ is given by assuming the following:

(i) the adsorbed Ar molecules are treated as a continuous liquid film adhered to the silica pore wall,

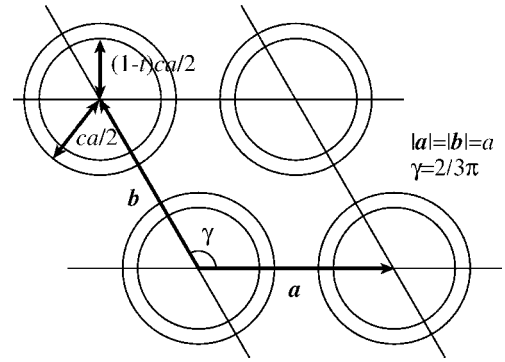

Figure 1. Structure model of MCM-41 with adsorbed gas on a 2D hexagonal lattice. During the gas adsorption procedure, the adsorbed film thickness $tca/2$ changes through the parameter t.

(ii) the density of the adsorbed film, as well as the density of the capillary condensate, equals the density of liquid Ar at a given temperature,

(iii) the adsorbed film has a uniform thickness, and

(iv) $\mathcal{F}[L_h(\mathbf{r})] \neq 0$ only at $\mathbf{k} = h\mathbf{a}^* + k\mathbf{b}^*$, where h and k are integers and $\mathbf{a}^*$ and $\mathbf{b}^*$ are reciprocal vectors ($|\mathbf{k}|a = 2[(h^2 + hk + k^2)/3]^{1/2}$).

Two cases, (a) and (b), should be considered separately:

(a) Mesopores are either completely filled with adsorbate after capillary condensation or completely empty:

$$C(\mathbf{r}) = \rho_{\text{wall}} \cdot S(\mathbf{r}) - (\rho_{\text{wall}} - \rho_{\text{pore}}) \cdot G(\mathbf{r}) * B(\mathbf{r}) * \{L_h(\mathbf{r}) \cdot S(\mathbf{r})\} \quad (3.3)$$

where ρ_{pore} is the interior density of the pore filled with Ar gas. If the pore interior is a vacuum, then $\rho_{\text{pore}} = 0$ and eq 3.3 will be the same as eq 3.2.

(b) Mesopores are partly filled with adsorbate:

$$C(\mathbf{r}) = \rho_{\text{wall}} \cdot S(\mathbf{r}) - G(\mathbf{r}) * \{(\rho_{\text{wall}} - \rho_{\text{pore}}) \cdot B(\mathbf{r}) + \rho_{\text{pore}} \cdot B_{\text{small}}(\mathbf{r})\} * \{L_h(\mathbf{r}) \cdot S(\mathbf{r})\} \quad (3.4)$$

where $B_{\text{small}}(\mathbf{r})$ is an empty cylinder with a diameter of $ca(1 - t)$, and t is the ratio of the adsorbed film thickness-to-pore radius, with $0 \leq t \leq 1$ (Figure 1).

We found in a previous paper[16] that the pore shape of calcined MCM-41 is circular. However, in this work we used another batch of samples, so first we checked whether a circle or a hexagon would be appropriate for the pore shape (the cross section of the channel) at 0 kPa. We then kept the pore shape constant for the whole Ar gas adsorption experiment and refined other structural parameters.

Therefore, the structure factor is obtained from eq 3.4 as

$$\begin{aligned}\mathcal{F}[C(\mathbf{r})] &= \rho_{\text{wall}} \cdot \mathcal{F}[S(\mathbf{r})] - \mathcal{F}[G(\mathbf{r})] \cdot \mathcal{F}[(\rho_{\text{wall}} - \rho_{\text{pore}}) \cdot B(\mathbf{r}) + \rho_{\text{pore}} \cdot B_{\text{small}}(\mathbf{r})] \cdot \mathcal{F}[L_h(\mathbf{r}) \cdot S(\mathbf{r})] \\ &= \rho_{\text{wall}} \cdot FS(h,k) - FG(h,k) \cdot [(\rho_{\text{wall}} - \rho_{\text{pore}}) \cdot FB(h,k) + \rho_{\text{pore}} \cdot FB_{\text{small}}(h,k)] \cdot FLS(h,k) \quad (3.5)\end{aligned}$$

It was confirmed that the sample size is large enough to assume to be infinite, thus, we consider only the intensity at $(h,k) \neq (0,0)$. Then, eq 3.5 can be simplified, as

$$\begin{aligned}F(h,k) &= -FG(h,k) \cdot [(\rho_{\text{wall}} - \rho_{\text{pore}}) \cdot FB(h,k) + \rho_{\text{pore}} \cdot FB_{\text{small}}(h,k)] \\ &= -FG(h,k) \cdot \rho_{\text{wall}}[(1 - \rho) \cdot FB(h,k) + \rho \cdot FB_{\text{small}}(h,k)] \quad (3.6)\end{aligned}$$

where h and k are integers, and $\rho = \rho_{\text{pore}}/\rho_{\text{wall}}$. The functions in

eq 3.6 are as follows:

For circular pores,

$$\mathcal{F}[B_{\text{small}}(\mathbf{r})] \equiv FB_{\text{small}}(h,k) = \left(\frac{a}{2}\right)^2 c(1-t)\sqrt{\frac{3}{h^2+hk+k^2}}J_1\left(2c(1-t)\pi\sqrt{\frac{h^2+hk+k^2}{3}}\right) \quad (3.7)$$

For hexagonal pores,

$$\mathcal{F}[B_{\text{small}}(\mathbf{r})] \equiv FB_{\text{small}}(h,k) = \left(\frac{a}{2}\right)^2 \Big[3\sqrt{3}\Big\{(h-k)\cos\frac{2\pi c(1-t)}{3}(h-k) - (2h+k)\cos\frac{2\pi c(1-t)}{3}(2h+k) + (h+2k)\cos\frac{2\pi c(1-t)}{3}(h+2k)\Big\}\Big] \Big/ [(h-k)(2h+k)(h+2k)\pi^2] \quad (3.8)$$

The other functions in eq 3.6 are described in a previous paper.[16]

Equation 3.6 gives the structure factor for Ar@MCM41 assuming the circular pores, and the full notation is

$$F(h,k) = -\left(\frac{a}{2}\right)^2 \exp[-(8/3)\pi^2\mu^2(h^2+hk+k^2)] \cdot c\sqrt{\frac{3}{h^2+hk+k^2}} \cdot \left[\begin{array}{l}(\rho_{\text{wall}}-\rho_{\text{pore}}) \cdot J_1\left(2c\pi\sqrt{\frac{h^2+hk+k^2}{3}}\right) \\ +\rho_{\text{pore}} \cdot (1-t) \cdot J_1\left(2c(1-t)\pi\sqrt{\frac{h^2+hk+k^2}{3}}\right)\end{array}\right] \quad (3.9)$$

The parameters for this equation are

- c the ratio of the pore size to the lattice parameter a ($0 \le c \le 1$),
- t the ratio of the adsorbed film thickness to the pore radius ($0 \le t \le 1$),
- ρ the scattering density ratio of adsorbed/condensed Ar to that of the silica wall, and
- μ the fluctuation parameter of the pore wall ($\mu \ge 0$).

At this stage, it will be usefull to show a general trend for discussion, which will be discussed in this paper. Figure 2a−c shows the dependence of diffraction intensities of 10- (a) and 11-, 20-reflections (b), and relative intensities of 11- and 20-reflections to that of 10-reflection (c) for the circular pore on the film thickness, t. The parameters are chosen as $a = 4$ nm, $c = 0.8$, $\rho = 0.5$, and $\mu = 0$. From Figure 2a,b, we can see the general trend of diffraction intensities of 10-, 11-, and 20-reflections as a function of film thickness ratio, t. The relative intensities of 11- and 20- reflections to that of 10-reflection is shown in Figure 2c, and it is clear from the model that the relative intensities give the same value for $t = 0$ and $t = 1.0$, as marked by arrows in Figure 2c, corresponding to the cases where the pore is completely empty and completely filled with adsorbate.

Assuming that the densities of the pore wall and the adsorbates inside the pore (ρ_{wall} and ρ_{pore}) are uniform, the crystal structure model for empty, without adsorbates, C_{Empty}, and fully filled, C_{Full}, pores are described as

$$\begin{cases} C_{\text{Empty}}(\mathbf{r}) = G(\mathbf{r}) * [\rho_{\text{wall}} - \rho_{\text{wall}} \cdot B(\mathbf{r}, ca)] \\ C_{\text{Full}}(\mathbf{r}) = G(\mathbf{r}) * [\rho_{\text{wall}} - (\rho_{\text{wall}} - \rho_{\text{pore}}) \cdot B(\mathbf{r}, ca)] \end{cases} \quad (3.10)$$

From these equations, the structure factors for empty and completely filled pores, are

$$\begin{cases} F_{\text{Empty}}(\mathbf{k}) = -\rho_{\text{wall}} \cdot FG(\mathbf{k}) \cdot FB(\mathbf{k}, ca) \\ F_{\text{Full}}(\mathbf{k}) = -(\rho_{\text{wall}} - \rho_{\text{pore}}) \cdot FG(\mathbf{k}) \cdot FB(\mathbf{k}, ca) \end{cases} \text{ for } \mathbf{k} \neq 0 \quad (3.11)$$

We assume here that the wall structure remains intact during the adsorption process, thus the product $FG(\mathbf{k}) \cdot FB(\mathbf{k},ca)$ is the same in both equations. The following equation is obtained:

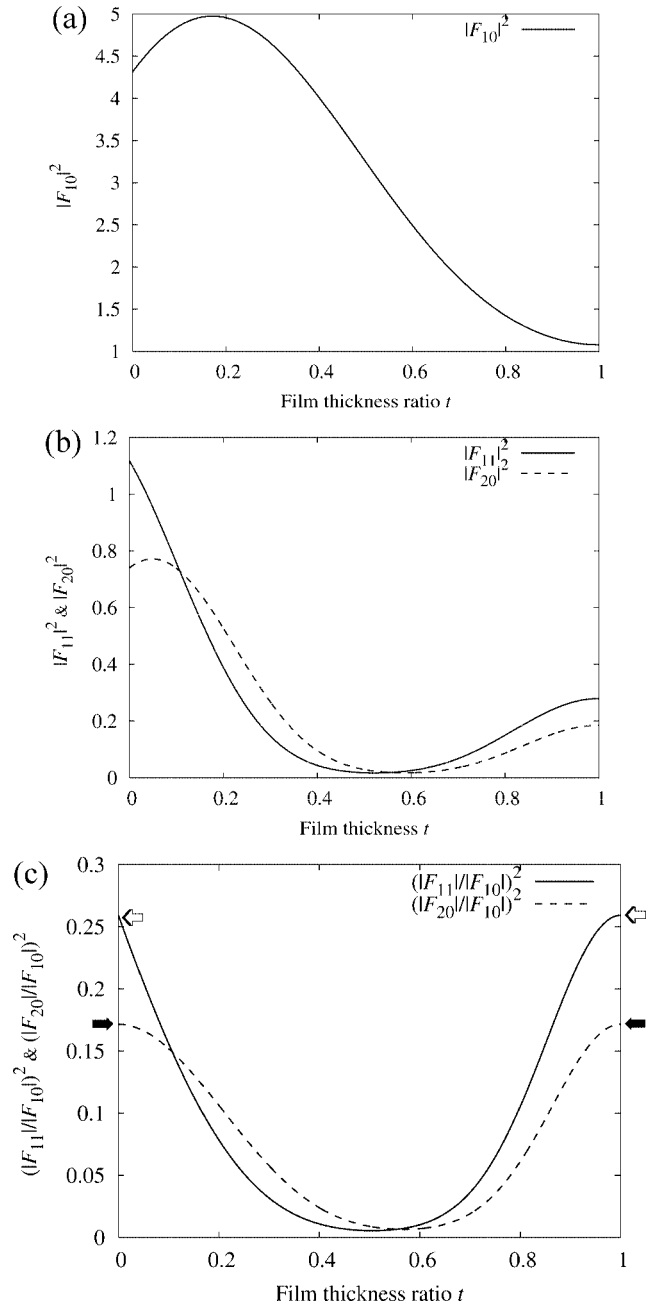

Figure 2. Diffraction intensity as a function of the film thickness t. Diffraction intensities of 10-reflection (a) and 11-, 20-reflections (b), and relative intensities of 11- and 20-reflections to that of 10-reflection (c). The parameters are set to be $a = 4$ nm, $c = 0.8$, $\rho = 0.5$, and $\mu = 0$.

$$\frac{F_{\mathrm{Full}}(\mathbf{k})}{F_{\mathrm{Empty}}(\mathbf{k})} = \frac{\rho_{\mathrm{wall}} - \rho_{\mathrm{pore}}}{\rho_{\mathrm{wall}}} = 1 - \rho\,, \quad \text{where} \quad \rho = \rho_{\mathrm{pore}}/\rho_{\mathrm{wall}} \tag{3.12}$$

We can obtain ρ from diffraction intensity by

$$\rho = 1 \pm \sqrt{\frac{|F_{\mathrm{Full}}(\mathbf{k})|^2}{|F_{\mathrm{Empty}}(\mathbf{k})|^2}} = 1 \pm \sqrt{\frac{I_{\mathrm{Full}}(\mathbf{k})}{I_{\mathrm{Empty}}(\mathbf{k})}} \tag{3.13}$$

This equation is valid for any structure models; it can be used for determining the adsorbate−solid density ratio.

Experimental Section

Synthesis of MCM-41 Crystal. MCM-41 was synthesized at 373 K following the procedure reported previously,[20] except that hexadecyltrimethylammonium bromide was used as the only structure-directing surfactant. Sodium silicate solution was employed as the silica source. The product was washed by slurring in an ethanol−hydrochloric acid mixture before calcination in air at 823 K.

Gas Adsorption Measurements. Nitrogen (at 77.4 K, liquid nitrogen) and argon (at 87.3 K, liquid argon) volumetric adsorption/desorption measurements were performed with an Autosorb-I-C instrument (Quantachrome Instruments, Boynton Beach, FL) equipped with high-precision pressure transducers (Baratron MKS), including 0.0001−1 Torr pressure transducers for low-pressure measurements. High-resolution data collection was performed in the relative pressure range P/P_0 from 2×10^{-6} to 1. The saturation pressure P_0 was measured throughout the entire analysis by means of a dedicated saturation pressure transducer. Low-pressure data points were corrected for the thermal transpiration effect according to a standard procedure.[21] The samples were outgassed overnight at 423 K prior to the adsorption analysis.

In Situ Powder XRD Intensity Measurements. Powder XRD experiments were performed by using synchrotron radiation at BL02B2 at SPring-8, Japan, and a Debye−Scherrer-type camera with an imaging plate. The experimental setup is shown in Figure 3, and more details can be found in our previous review paper.[22] The wavelength used was determined to be 0.100 nm. The specimen was mounted in a fused soda capillary with a diameter of 0.3 mm, and was kept at ca. 85 K by using N_2 gas flow from a liquid N_2 reservoir. The sample was pre-evacuated at 450 K for 10 min before starting a series of experiments, and Ar-gas pressure was changed stepwise manually and maintained for ca. 10 min to obtain equilibrium conditions before the XRD measurement. In order to scale the measured intensities, two approaches, (i) time of exposure and (ii) integrated scattered intensity from the internal standard, were used. α-Al_2O_3 fine powder from NIST SRM 674a was used as the internal standard for the following reasons: (i) it is very crystalline, (ii) it is a good standard for calibrations of scattered intensity and deviation of the origin in the imaging plate, (iii) it has small adsorption for X-ray, and (iv) it exhibits almost no Ar adsorption.

Results and Discussions

1. Adsorption. The Ar adsorption−desorption isotherm at 87.3 K on the calcined MCM-41 sample is given in Figure 4a. The isotherm demonstrates a sharp step, characteristic of the capillary condensation in cylindrical mesopores, and a flat hysteresis loop originated from irreversible condensation occurring near the saturation pressure in some wide cavities, which are not relevant to our analysis. Two runs show a reproducibility of adsorption measurements. The N_2 adsorption isotherm at 77.4 K (not shown) exhibited similar features. The pore size distribution (PSD) was calculated by the nonlocal density functional theory (NLDFT) method,[23] which is incorporated into the Quantachrome Instruments software. The PSD obtained from the Ar isotherm is given in Figure 4b. It exhibits a narrow distribution of pore diameters around 4.0 ± 0.2nm. Almost identical PSD (not shown) was obtained from the N_2 adsorption isotherm at 77.4 K. Note that the pore diameter defined in the NLDFT method represents the internal diameter counted from the edges of the outer oxygen atoms in the silica wall. It differs by 0.27 nm from the pore diameter defined as the distance between the centers of the outer oxygen atoms in the silica wall. Thus, the internal pore diameter determined by NLDFT should correspond to the

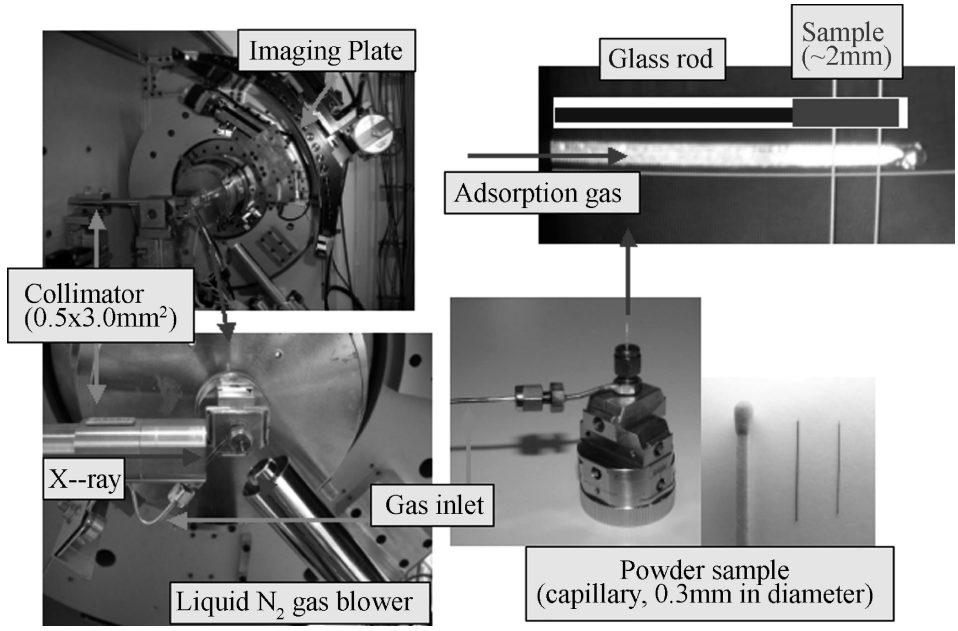

Figure 3. Set-up for in situ gas adsorption XRD experiment at Spring-8.

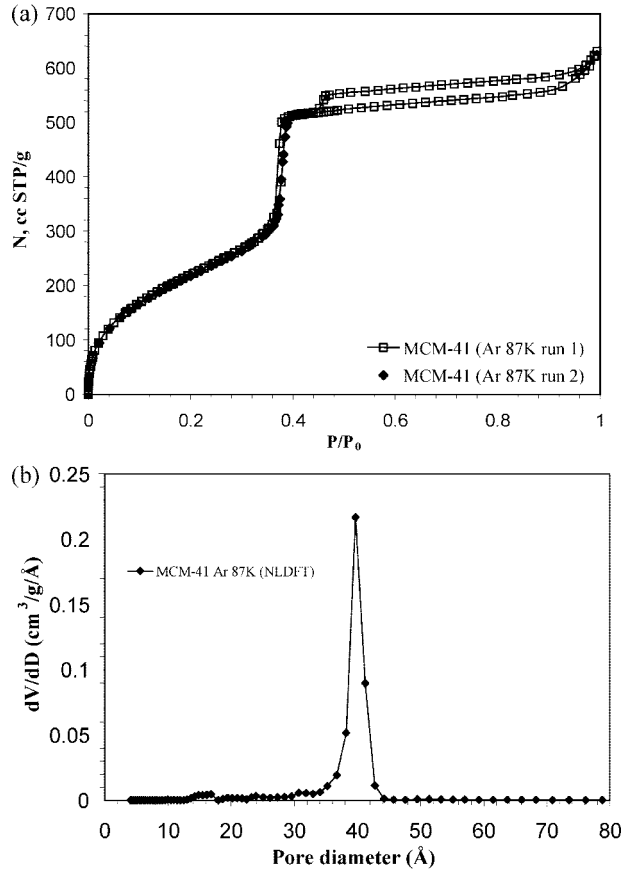

Figure 4. (a) Ar-gas adsorption isotherm at 87 K, and (b) pore distribution curve obtained from NLDFT analysis.

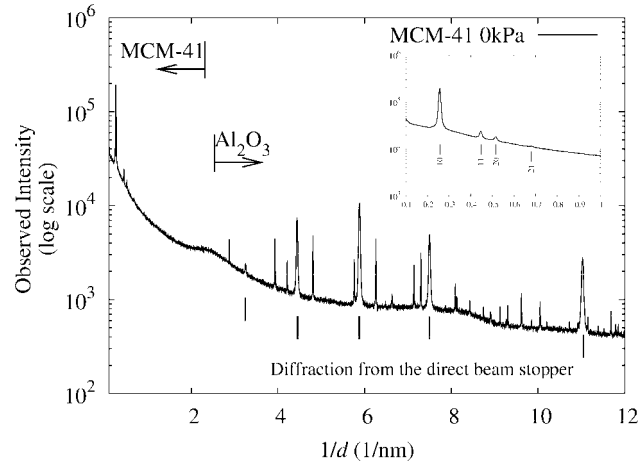

Figure 5. A powder diffraction profile of MCM-41 with α-Al_2O_3 at 0 kPa (b).

pore diameter defined from the electron density distribution obtained in XRD measurements.

2. XRD. Figure 5 shows the powder XRD pattern of the calcined MCM-41 at 0 kPa. We can observe diffraction peaks both from silica mesoporous MCM-41 and from finely powdered α-Al_2O_3 well-separated in scattering angle range without any interferences. Diffraction peaks from the direct-beam stopper were also observed, and are marked by vertical lines. Each measurement at different gas loading was taken under the different measurement time.

Observed patterns were analyzed by the following steps:

1. Analyze the diffraction patterns of the internal standard by the Rietveld method to obtain the scale factor at each gas pressure.
2. At each gas pressure, obtain integrated intensities and the unit cell length of MCM-41 by individual profile fitting.
3. Determine the pore shape of MCM-41 at 0 kPa.
4. Calculate the density ratio of the pore to the silica wall, ρ, by the model free method, which uses eq 3.13 as the initial value for the refinement of step 5.
5. With the data of all gas pressures, to refine the all parameters, that is, ρ, the adsorbed film thickness, t, the pore size ratio to the unit cell length, c, and the fluctuation parameter, μ.

In the following, each step is explained in detail.

Step 1. The diffraction pattern of the internal standard, α-Al_2O_3, is analyzed by the Rietveld method in order to obtain the scale factor. The Rietveld analysis software was programmed by Y.K., and the profile function is the split-type Pearson VII function. The scale factors obtained from this analysis are shown together with the measurement times in Table 1. Good correspondence between the scale factors and measurement times was confirmed, and the scale factors obtained here are used for the following refinement.

Step 2. Profile fitting with split-type Pearson VII function is used to obtain the integrated intensity and the peak position of each reflection of MCM-41 at different gas pressures. The unit cell parameter is calculated by the least-squares method with all peak positions at each gas pressure. The integrated intensities for all reflections were corrected with the scale factor and the Lorentz polarization factor. The unit cell parameter and $|F(\mathbf{k})|^2$ for all reflections are also shown in Table 1. XRD patterns after all corrections are shown in Figure 6 as a function of gas pressure. $|F(\mathbf{k})|^2$ for 10-reflection and 11-, 20-reflections are shown in Figure 7a,b, respectively, at all gas pressures. $|F(\mathbf{k})|^2$ for the 10-reflection dramatically changed between 15 kPa and 18 kPa. This change is caused by the sharp uptake due to the capillary condensation and the corresponding increase of the effective thickness of the adsorbed layer up to its limiting value equal to the pore radius achieved upon the complete pore filling by the liquid-like Ar. $|F(\mathbf{k})|^2$ for the 11- and 20-reflections crosses at the same gas pressure between 15 kPa and 18 kPa. The dependence of the unit cell parameter on the gas pressure is shown in Figure 8. The unit cell parameter is almost constant at different gas pressures, although data points are scattered a little (error bars are 1σ and 3σ). We found that the unit cell parameter is hardly related to the gas pressure, and therefore we fix the unit cell constant to the value obtained at 0 kPa in the following analysis.

Step 3. The pore shape, pore diameter parameter c, and the fluctuation parameter μ were obtained from the XRD pattern at 0 kPa, and the analysis procedure is the same as in the previous paper. The pore shape was circular as in the previous paper and fixed in the further analysis. The parameters c and μ obtained here are the initial parameters and are further refined at step 5.

Step 4. In this experiment, we have one data point at 0 kPa for the case for empty pores and three data points at 30, 40, and 50 kPa for the completely filled pores. Figure 9 shows XRD patterns observed from the cases of empty pore (0 kPa) and of completely filled pore (as an example, 50 kPa). The left-hand values of eq 3.12 are calculated for 30, 40, and 50 kPa and averaged. The ρ is calculated from eq 3.13 and is 0.56 or 1.45. In this experiment, the density of the silica wall is larger than that of the Ar film density, therefore $\rho = 0.56$ is a proper value.

TABLE 1: The Exposure Time of XRD, the Scale Factor Obtained from the Analysis of Integrated Intensities of Al_2O_3, the Unit Cell Parameter of MCM-41, and the Structure Factors of MCM-41 with Adsorbed Ar at Each Gas Pressure

pressure (kPa)	time (min)	scale factor	unit cell parameter (nm)	$\|F(1,0)\|^2$	$\|F(1,1)\|^2$	$\|F(2,0)\|^2$	$\|F(2,1)\|^2$
0	15	0.1009(4)	4.475(2)	0.4338(14)	0.0672(19)	0.0395(19)	0.0032(9)
3	15	0.0985(6)	4.480(5)	0.552(2)	0.037(3)	0.038(3)	
6	15	0.1017(5)	4.484(6)	0.5496(19)	0.025(2)	0.031(2)	
9	15	0.1044(6)	4.480(8)	0.5413(19)	0.019(2)	0.026(3)	
12	15	0.1061(6)	4.488(11)	0.523(2)	0.013(3)	0.021(3)	
15	15	0.1097(4)	4.475(15)	0.4537(18)	0.009(2)	0.015(2)	
18	15	0.1016(5)	4.470(8)	0.1677(7)	0.0114(11)	0.0100(12)	
21	30	0.2076(11)	4.483(5)	0.0933(5)	0.0127(8)	0.0090(9)	
25	30	0.2112(10)	4.498(6)	0.1217(7)	0.0133(10)	0.0101(12)	
30	45	0.2991(17)	4.469(4)	0.0835(3)	0.0175(7)	0.0088(7)	
40	45	0.2932(16)	4.485(5)	0.0862(4)	0.0180(8)	0.0109(8)	
50	60	0.398(2)	4.475(3)	0.0866(5)	0.0156(8)	0.0085(8)	

The values obtained from the data for the empty and completely filled states, a, c, μ, and ρ are used as the initial values for the further refinement.

Step 5. Three reflections were observed in each Ar-gas pressure except for four peaks at 0 kPa, and the total number of observed peaks is 37. To obtain the parameters with the nonlinear least-squares methods, all parameters are refined simultaneously except for the adsorbed film thickness, t, which is kept fixed to zero at 0 kPa. After the first refinement, the residual, which is defined as $\sum(I_{cal} - I_{obs})^2/\sum I_{obs}^2$, is 2.65%, and t values at 30, 40, and 50 kPa are quite close to 1.0. We assumed that capillary condensation was completed at 30, 40 and 50 kPa and fixed the value t to 1 at 30, 40, and 50 kPa for the next refinement, although the observed intensity and therefore the analysis results at 25 kPa somewhat deviated from the smooth variation of the points obtained at other pressures. The final results are shown in Tables 2 and 3, and the residual for this result is 2.44%. Figure 10 shows the observed dependence of the thickness of adsorbed film on a function of the gas pressure. We define the pressure for capillary condensation by the inflection point of this curve, which corresponds to ca. 0.5 of the film thickness t.

3. QSDFT. In an attempt to predict the results of the in situ XRD measurements of the thickness of adsorbed layer and the position of capillary condensation, we have performed the following calculations. Our initial input data was the adsorption isotherm of Ar measured at 87.3 K. Since the XRD measurements were done at a lower temperature, we first had to reproduce the adsorption isotherm at the conditions of the XRD experiment. The sample temperature in the XRD unit was experimentally estimated to be ~85 K. However, this temperature was measured outside the test tube with the sample, and we assume that, since the cooling was provided with a spray of liquid nitrogen (77.4 K), the sample temperature might have been somewhat lower than 85 K. Adsorption is very sensitive to temperature, so even a small error in temperature (1−2°) may lead to unacceptable deviations in calculated adsorption isotherms. This is why we have chosen the experimental pressure of capillary condensation (16.3 kPa), rather than the

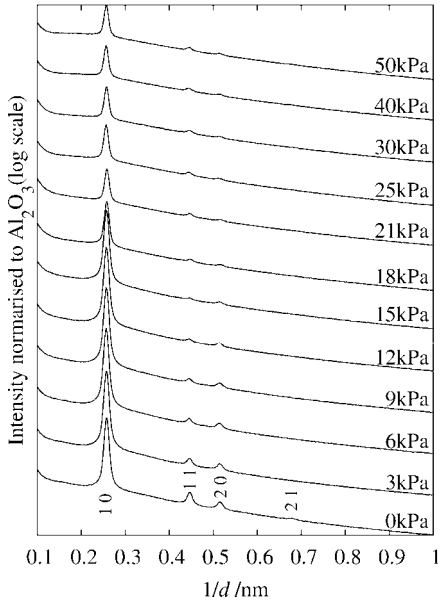

Figure 6. XRD patterns after being normalized using the internal intensity standard of α-Al_2O_3.

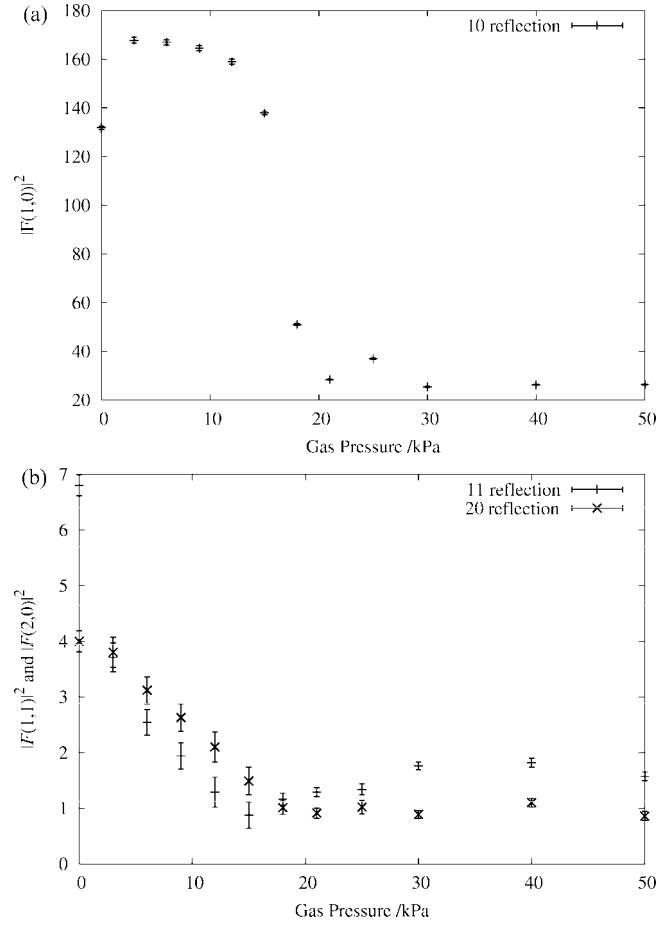

Figure 7. The dependence of $|F|^2$ on gas pressure for (a) 10-, and (b) 11-, 20- reflections, respectively.

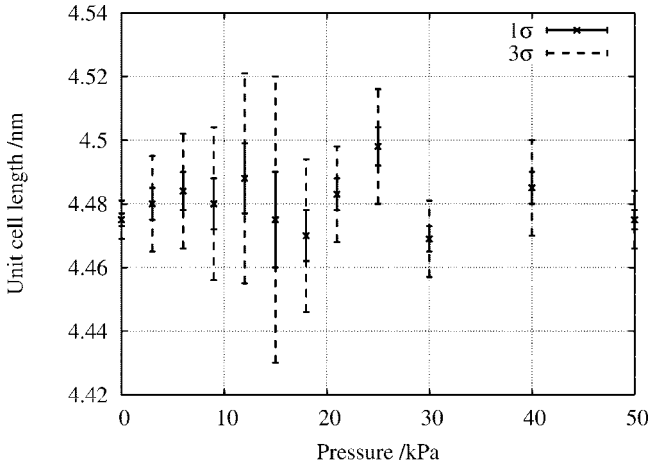

Figure 8. The unit cell parameter of MCM-41 with adsorbed Ar as a function of the gas pressure.

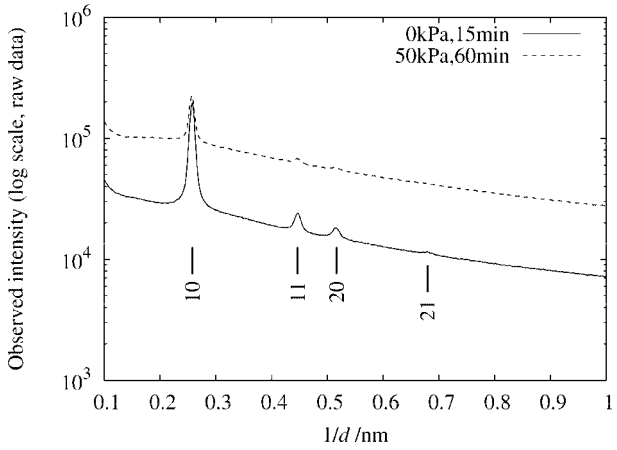

Figure 9. XRD patterns as observed for 0 kPa and 50 kPa. The exposure times were 15 and 60 min for 0 kPa and 50 kPa, respectively. Right ordinate corresponds to the degree of pore filling, N/N_o, calculated from the film thickness, t, by eq 4.4.

TABLE 2: The Refined Parameters, ρ_{pore}/ρ_{wall}, the Pore Size, Fluctuation Parameter, and Thickness of Adsorbed Film at Each Gas Pressure.

pressure (kPa)	density ratio ρ_{pore}/ρ_{wall}	pore size c	fluctuation μ	film thickness ratio t
0	0.5586(8)	0.8218(11)	0.0699(10)	0
3				0.177(8)
6				0.205(8)
9				0.235(7)
12				0.283(5)
15				0.385(3)
18				0.7161 (14)
21				0.908(3)
25				0.808(2)
30				1
40				1
50				1

temperature, as the external thermodynamic parameter characterizing the conditions of the XRD experiment. To appreciate the crucial role of temperature, this pressure should be compared with the pressure of 38.3 kPa, at which the capillary condensation occurred during adsorption measurements at 87.3 K.

For calculations of adsorption isotherms, we employed the QSDFT model developed recently to study adsorption in silica pores with molecularly rough silica walls.[19] This model presents the silica wall as having a diffuse layer (corona) of spatially

TABLE 3: Silica Density[a]

	ρ_{pore}/ρ_{wall}	SiO2 (g/cm^3)
Refinment	0.5586(8)	2.247(3)
Model free	0.5569(18)	2.254(7)

[a] The model free is calculated by eq. 3.11.

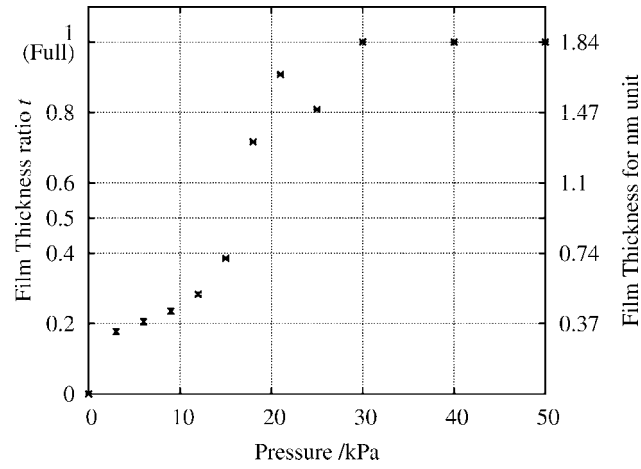

Figure 10. The thickness of adsorbed film as a function of the Ar-gas pressure. The ratio of the adsorbed film thickness to the pore radius, t, is shown. The film thickness $tca/2$ (see Figure 1) is given in nanometer units. NB Ar atomic radius = 0.19 nm.

distributed density of solid atoms, which is lower than the density of the bulk silica. In this work, the solid density in this diffuse layer was distributed in accord with a linear ramp function:

$$\rho_s = \begin{cases} 0 & \text{at } r < R_c - \delta \\ \rho_{s0}(r - R_c + \delta)/2\delta & \text{at } R_c - \delta < r < R_c + \delta \\ \rho_{s0} & \text{at } r > R_c + \delta \end{cases} \quad (4.1)$$

Here, R_c is the geometrical mean radius, δ is the roughness parameter defined as the semiwidth of the ramp, and ρ_{s0} is the density of the bulk solid. To reproduce the experimentally measured isotherm at 87.3 K, we have chosen the model of the silica pore with the geometrical mean radius of $R_c = 2.11$ nm and the roughness parameter $\delta = 0.4$ nm. In the cylindrical geometry, one can define the effective pore radius R_S, which corresponds to zero excess mass of solid, according to

$$\frac{\rho_{S0}}{2\delta}\int_{R_C-\delta}^{R_C+\delta} 2\pi r(r - R_C + \delta)\mathrm{d}r = \pi\rho_{S0}((R_C + \delta)^2 - R_S^2) \quad (4.2)$$

$$R_S = R_C(1 + (\delta/R_C)^2/3)^{1/2} \quad (4.3)$$

The obtained R_S is equal to 2.12 nm, and, after subtracting the oxygen atom diameter of 0.27 nm, the internal pore diameter of the pore agrees with the mean internal pore diameter determined by the NLDFT method. The roughness parameter δ is in reasonable agreement with the fluctuation parameter μ employed in the XRD calculations. However, a direct relationship between these two parameters has still to be discussed. We refer the reader to reference 19 for a detailed description of QSDFT, the parameters of interaction potentials, and the computational scheme employed.

The results of QSDFT calculations of Ar adsorption isotherms are presented in Figure 11. The agreement with the experimental Ar isotherm at 87.3 K is excellent, which validates the choice of the model parameters. We found by computing a series of

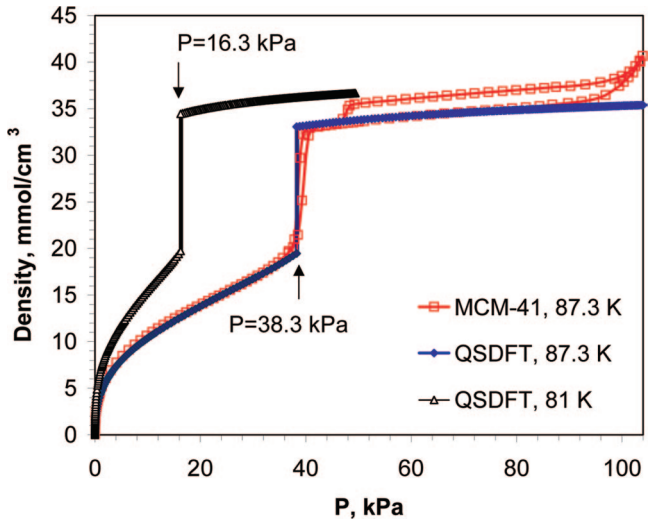

Figure 11. Capillary condensation of Ar in the cylindrical pore of MCM-41. The experimental isotherm at 87.3 K is compared with the QSDFT model calculations. The same QSDFT model was used to predict adsorption at 81 K. The equilibrium transition pressure at 81 K is 16.3 kPa.

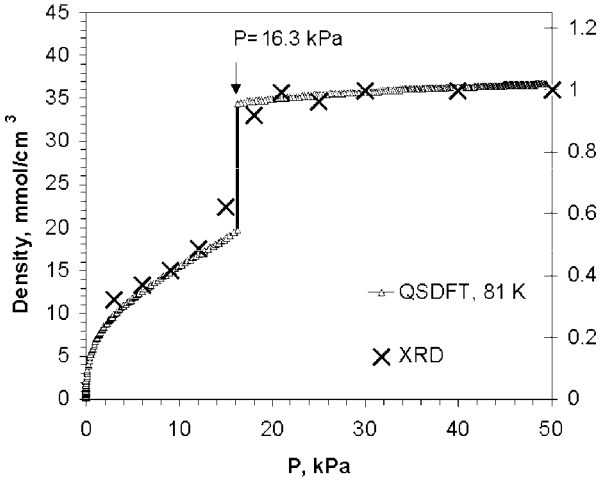

Figure 12. Prediction of adsorption isotherm at 81 K in comparison with the isotherm calculated from the XRD film thickness.

QSDFT isotherms at different temperatures that, within the accepted pore model, the capillary condensation pressure of 16.3 kPa, which is an XRD experiment result, is predicted at 81 K. This suggests that the adsorption process under the conditions of the XRD experiment can be described with the QSDFT model as occurring at 81 K.

Discussion

In Figure 12, we compare the adsorption isotherm predicted by QSDFT at 81 K with the XRD data directly recalculated from the values of the adsorbed film thickness reported in Table 2. The XRD adsorption isotherm was calculated as the degree of pore filling defined as the adsorption N at a given relative pressure reduced to the adsorption at the conditions of the complete pore filling N_0. Taking into account that the adsorbed film in the model employed for the interpretation of the XRD data is assumed to be a uniform cylindrical layer of the liquid Ar density, we come to the following simple formula:

$$N/N_0 = 1 - (1 - t)^2 \quad (4.4)$$

A perfect agreement of the QSDFT predicted isotherm and the XRD recalculated isotherm suggests that the adsorption porosimetry and XRD measurements can be reconciled provided a proper interpretation of the experimental data.

In Figure 13, we present the evolution of the adsorbed Ar density as the vapor pressures increases. The QSDFT calculations predict the formation of the adsorbed film following the complete pore filling due to capillary condensation, thus confirming the general scenario of the adsorption process.

In Figure 14a, the Ar density profiles predicted by QSDFT and the solid density profiles are recalculated in terms of the electron density profiles. It should be mentioned that the electron density profiles were converted from the corresponding density profiles predicted by QSDFT by convolving an electron cloud to them. We used the simplest rigid-like electron spreads $3N_e\theta(s - |\mathbf{r}|)/4\pi s^3$, where N_e is the number of electrons, s is the van der Waals radius of the relevant atoms, and θ represents the Heaviside theta function. Figure 14b allows the direct comparison of the theoretical results originating from the analysis of adsorption data with the experimental XRD data interpreted in accord with the proposed method. The electron density profiles calculated from the XRD patterns are given in Figure 14b. This is calculated by the following formula:

$$\frac{1}{(\mu a)^2}\int_{r_1}^{r_2} r' \cdot \exp\left[-\frac{r^2 + r'^2}{2(\mu a)^2}\right] \cdot I_0\left[\frac{r \cdot r'}{(\mu a)^2}\right] dr'$$

where r and r' are the radial coordinates, and I_0 represents the modified Bessel function with the zeroth order. The charge density distribution in the center of the pore from XRD calculation is different from that of the QSDFT model, since the XRD model assumes a gas film, even after capillary condensation. Although the theoretical and the experimental profiles do not coincide perfectly, the agreement is truly amazing, taking into account the assumptions employed in the calculations.

It is natural that the dependence of the adsorbed film thickness, t, on the gas pressure obtained from the in situ XRD experiment is similar to that of the adsorption isotherm. However, the pressure where the capillary condensation takes place is different between the two experiments.

This can be explained by the fact that the experimental temperature of the in situ XRD intensity measurement may be lower than 85 K and be close to 81 K, as estimated from the QSDFT model. The pore diameters obtained from the in situ XRD experiment and the Ar gas adsorption isotherm experiment are 3.7 and 4.0 nm, respectively. This discrepancy should be studied further.

If we determine that capillary condensation starts at $t = 0.5$, then capillary condensation starts at a pore diameter of 1.8 nm with a thickness of Ar-atom layer of 0.9 nm at 90 K. If the atomic radius of an Ar atom is taken to be the van der Waals radius (0.19 nm), the Ar atoms form a single layer at 3 kPa, and then the thickness of the Ar atoms increases with Ar-gas pressure. At ca. 15 kPa, capillary condensation starts at a thickness of 2.3 layers of Ar-atoms.

Conclusion

In situ powder XRD measurement allowed the determination of the pore structure and the specifics of the adsorption process on the basis of the theoretical analysis, which takes into account the changes in the electron density of the crystal due to accumulation of adsorbed fluid. The theoretical description of

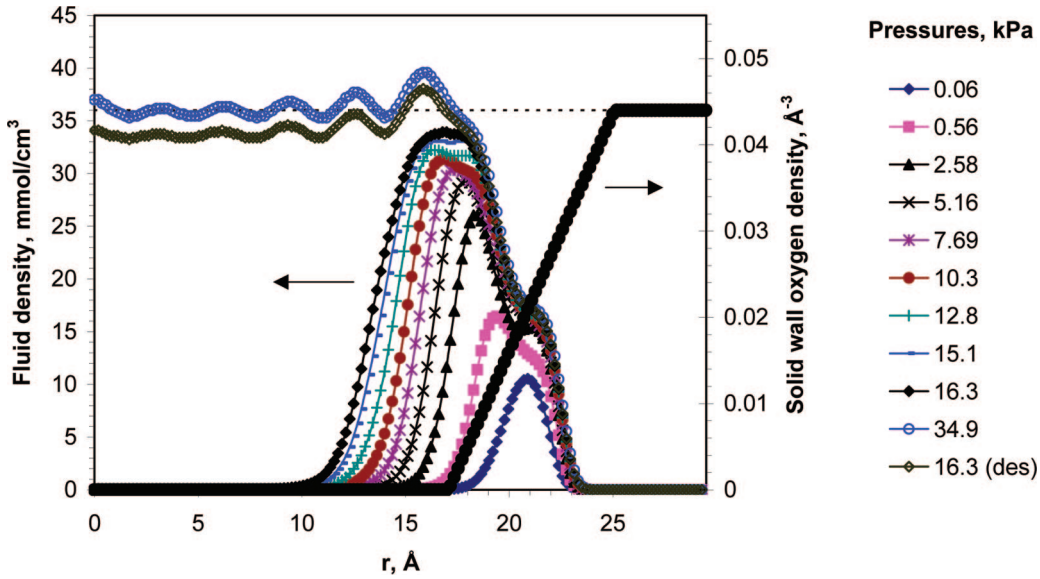

Figure 13. QSDFT density profiles of Ar at 81 K in the cylindrical pore of MCM-41 at different pressures. The radial coordinate r is measured from the center of the cylindrical pore. The dotted horizontal line corresponds to the bulk liquid density of supercooled Ar at 81 K (~36 mmol/cm^3). The silica surface is modeled as a diffuse interface, the roughness of which is characterized by the density distribution of oxygen atoms in the diffuse layer in the form of a linear ramp with the center at $r = R_c = 2.11$ nm and the roughness parameter $\delta = 0.4$ nm. The effective internal pore diameter is 3.97 nm as determined by the NLDFT method. The bulk number density of oxygen atoms in silica is 0.044 Å^{-3}, which corresponds to the silica density of 2.2 g/cm^3.

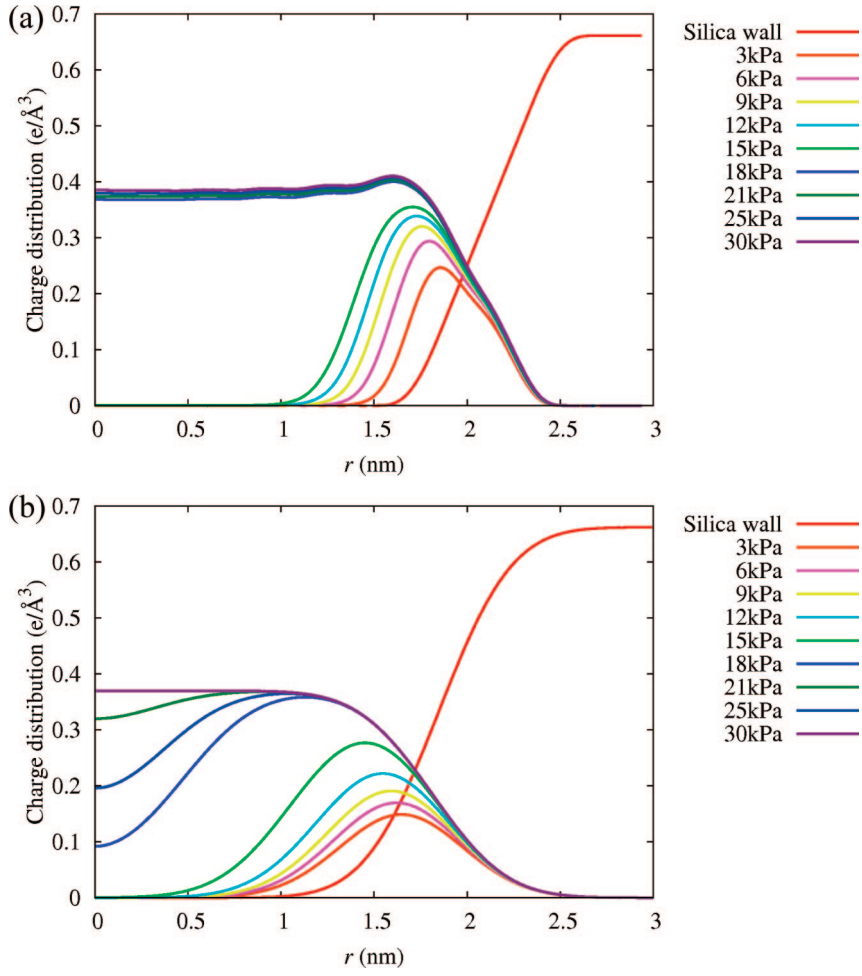

Figure 14. (a) The electron density profiles predicted by the QSDFT model at 81 K. A rigid-like electron spread was convolved to the density profiles in the QSDFT calculation. (b) The electron density profiles calculated from XRD patterns.

the adsorption process by means of the QSDFT is in overall good agreement with data obtained from in situ XRD and adsorption measurements, including the electron/atom density profiles, the surface fluctuation/roughness parameters, and the

adsorption isotherm expressed as a variation of the film thickness with the gas pressure.

Acknowledgment. Financial support from the Swedish Research Council (VR) and Japanese Science and Technology Agency (JST) are acknowledged. This study was partly supported by a Grant-In-Aid for Science Research from the Ministry of Education, Culture, Sports, Science and Technology of Japan. This study was also supported by JASRI/SPring-8 Nanotechnology Support Project of the Ministry of Education, Culture, Sports, Science and Technology of Japan. The authors thank Drs. K. Kato and K. Osaka of JASRI for their kind advice and help in data collection. R.R. acknowledges support from the Ministry of Education, Science, and Technology through the National Honor Scientist Program. A.N.V. acknowledges a grant from Quantachrome Instruments and thanks Dr. M. Thommes for fruitful discussions.

References and Notes

(1) Yanagisawa, T.; Shimizu, T.; Kuroda, K.; Kato, C. *Bull. Chem. Soc. Jpn.* **1990**, *63*, 988.

(2) Kresge, C. T.; Leonowicz, M. E.; Roth, W. J.; Vartuli, J. C.; Beck, J. S. *Nature* **1992**, *359*, 710.

(3) Zhao, D. Y.; Feng, J. L.; Huo, Q. S.; Melosh, N.; Fredrickson, G. H.; Chmelka, B. F.; Stucky, G. D. *Science* **1998**, *279*, 548.

(4) Che, S.; Garcia-Bennett, A. E.; Yokoi, T.; Sakamoto, K.; Kunieda, H.; Terasaki, O.; Tatsumi, T. *Nat. Mater.* **2003**, *2*, 801.

(5) Beck, J. S.; Vartuli, J. C.; Roth, W. J.; Leonowicz, M. E.; Kresge, C. T.; Schmitt, K. D.; Chu, C. T. W.; Olson, D. H.; Sheppard, E. W.; Mccullen, S. B.; Higgins, J. B.; Schlenker, J. L. *J. Am. Chem. Soc.* **1992**, *114*, 10834.

(6) Carlsson, A.; Kaneda, M.; Sakamoto, Y.; Terasaki, O.; Ryoo, R.; Joo, S. H. *J. Electron Microsc.* **1999**, *48*, 795.

(7) Sakamoto, Y.; Kaneda, M.; Terasaki, O.; Zhao, D. Y.; Kim, J. M.; Stucky, G.; Shim, H. J.; Ryoo, R. *Nature* **2000**, *408*, 449.

(8) Edler, K. J.; Reynolds, P. A.; White, J. W.; Cookson, D. *J. Chem. Soc., Faraday Trans.* **1997**, *93*, 199.

(9) Solovyov, L. A.; Kirik, S. D.; Shmakov, A. N.; Romannikov, V. N. *Microporous Mesoporous Mater.* **2001**, *44*−*45*, 17.

(10) Morishige, K.; Tateishi, M. *Langmuir* **2006**, *22*, 4165.

(11) Mitropoulos, A. C.; Haynes, J. M.; Richardson, R. M.; Kanellopoulos, N. K. *Phys. Rev. B* **1995**, *52*, 10035.

(12) Albouy, P. A.; Ayral, A. *Chem. Mater.* **2002**, *14*, 3391.

(13) Pikus, S.; Solovyov, L. A.; Kozak, M.; Jaroniec, M. *Appl. Surf. Sci.* **2007**, *253*, 5682.

(14) Imperor-Clerc, M.; Davidson, P.; Davidson, A. *J. Am. Chem. Soc.* **2000**, *122*, 11925.

(15) Zickler, G. A.; Jahnert, S.; Wagermaier, W.; Funari, S. S.; Findenegg, G. H.; Paris, O. *Phys. Rev. B* **2006**, *73*, 184109.

(16) Muroyama, N.; Ohsuna, T.; Ryoo, R.; Kubota, Y.; Terasaki, O. *J. Phys. Chem. B* **2006**, *110*, 10630.

(17) Kaneda, M.; Tsubakiyama, T.; Carlsson, A.; Sakamoto, Y.; Ohsuna, T.; Terasaki, O.; Joo, S. H.; Ryoo, R. *J. Phys. Chem. B* **2002**, *106*, 1256.

(18) Liu, Z.; Sakamoto, Y.; Ohsuna, T.; Hiraga, K.; Terasaki, O.; Ko, C. H.; Shin, H. J.; Ryoo, R. *Angew. Chem., Int. Ed.* **2000**, *39*, 3107.

(19) Ravikovitch, P. I.; Neimark, A. V. *Langmuir* **2006**, *22*, 11171.

(20) Kruk, M.; Jaroniec, M.; Sakamoto, Y.; Terasaki, O.; Ryoo, R.; Ko, C. H. *J. Phys. Chem. B* **2000**, *104*, 292.

(21) Neimark, A. V.; Ravikovitch, P. I.; Grun, M.; Schuth, F.; Unger, K. K. *J. Colloid Interface Sci.* **1998**, *207*, 159.

(22) Kubota, Y.; Takata, M.; Kobayashi, T. C.; Kitagawa, S. *Coord. Chem. Rev.* **2007**, *251*, 2510.

(23) Neimark, A. V.; Ravikovitch, P. I. *Microporous Mesoporous Mater.* **2001**, *44*, 697.

JP800385T